Coastal landfast sea ice decay and break-up in northern Alaska: Key processes and seasonal prediction

Journal of Geophysical Research, doi:10.1029/2011JC007339, in press.

Chris Petrich
Geophysical Institute,
University of Alaska Fairbanks, Fairbanks, Alaska
Corresponding author email: chris.petrich@gi.alaska.edu

Hajo Eicken
Geophysical Institute and International Arctic Research Center
University of Alaska Fairbanks, Fairbanks, Alaska

Jing Zhang
Department of Physics and Energy & Environmental Systems
North Carolina A&T State University, Greensboro, North Carolina

Jeremy Krieger
Arctic Region Supercomputing Center
University of Alaska Fairbanks, Fairbanks, Alaska

Yasushi Fukamachi
Institute of Low Temperature Science
Hokkaido University, Sapporo, Japan

Kay I. Ohshima
Institute of Low Temperature Science
Hokkaido University, Sapporo, Japan

Three main points of the article, 80 characters max:

- Two break-up modes can be distinguished, differing in decay process and timing
- Significance of oceanic and atmospheric dynamics depends on break-up mode
- Break-up prediction is possible based on irradiance for the majority of years

Abstract

Seasonal break-up of landfast sea ice consists of movement and irreversible ice detachment in response to winds or oceanic forces in the late stages of ice decay. The break-up process of landfast sea ice in the Chukchi Sea at Barrow, Alaska was analyzed for the years 2000 through 2010, based on local observations of snow and ice conditions, weather records, image sequences obtained from cameras, coastal X-band marine radar, and satellite imagery. We investigated the relation of break-up to winds, tides, and near-shore current measurements from a moored Acoustic Doppler Current Profiler (ADCP). Two break-up modes are distinguished at Barrow based on the degree of ice decay. Mechanical break-up due to wind and oceanic forces follows ablation and weakening of the ice. Thermal break-up is the result of ice disintegration under melt ponds, requiring little forces to induce dispersion. Grounded pressure ridges are pivotal in determining the break-up mode. The timing of thermal break-up of the near-shore ice cover was found to correlate with the measured downwelling solar radiation in June and July. This linkage allows for the development of an operational forecast of landfast ice break-up. Results from forecasts during two years demonstrate that thermal break-up can be predicted to within a couple of days two weeks in advance. The cumulative shortwave energy absorbed by the ice cover provides for a measure of the state of ice decay and potential for disintegration. Discriminating between the two modes of break-up bears the potential to greatly increase forecasting skill.

1 Introduction

Much of the Arctic Ocean is ringed by a belt of landfast sea ice, typically a few kilometers to more than 100 km in width. Land- or shorefast ice protects the coast from the erosive impacts of storms and drifting pack ice [*Reimnitz et al.*, 1994]. It is an important habitat for organisms ranging from ice algae to seals and polar bears, providing a platform for feeding, breeding and resting [*Bluhm and Gradinger*, 2008]. Landfast ice also plays an important role in the life of Arctic communities, both for travel and hunting, as well as in the context of resource development as an operations platform [*Gearheard et al.*, 2006; *Aporta*, 2009; *Eicken et al.*, 2009]. At the same time, the presence of landfast ice in late spring limits access to the coastal ocean for hunters and boat travel. Thus, spring landfast ice break-up, either through dispersal or in-situ melt, is one of the most important events in the seasonal cycle of coastal environments. It greatly increases access to the coast and adjacent open waters, forces marine mammals with a preference for sea ice platforms offshore and increases the vulnerability of the shoreline to erosive action.

Tracking the timing of break-up on timescales of decades is hence crucial to assess the impacts of climate variability and change on ecosystems and human activities. Moreover, forecasting of break-up, even on timescales of days to a few weeks can be of potential value in preparing for the transition between ice- or landbased winter activities and ocean-based summer activities, whether from the perspective of a coastal village or an industrial operator. Finally, such forecasts may also be useful in the context of management of marine resources, in particular threatened or endangered species such as walrus or polar bears.

Break-up of landfast sea ice in the North American Arctic has been studied mostly in the context of ice trafficability and offshore oil and gas development [e.g., *Sackinger and Rogers*, 1974; *Spedding*, 1983; *Barry et al.*, 1979] or coastal dynamics [*Short and Wiseman*, 1975; *Shapiro and Barnes*, 1991]. The analysis of break-up in these studies was typically constrained by the types of observations (ground-based, remote sensing) available for a particular location, with little intercomparison between different types of observations and very few long-term studies of changes in break-up dates. Recent work by *Mahoney et al.* [2007a] provided an update on earlier work for the Chukchi and Beaufort Seas but relied exclusively on remote-sensing observations with data acquired at 10-day intervals.

For the Siberian Arctic, studies of the mechanisms of ice break-up have led to the development of simple forecast models [e.g., *Spichkin*, 1961; *Gudkovich*, 1995]. As summarized by *Gudkovich* [1995], warming and ablation (decay) precondition the

landfast ice for break-up under the influence of dynamic forces of winds and ocean. In the Siberian Arctic, semi-empirical approaches have been employed that rely on one or several factors, such as air temperature, wind speed and ice thickness to predict break-up on timescales of days to a few weeks. While we were not able to find comparisons between model forecasts and observations, Gudkovich specifies predictive success relative to climatology at 20 to 35%. For the Alaskan Beaufort Sea coast, *Barry et al.* [1979] state that 55 to 140 and 140 to 220 melting degree days (MDD) are required to observe opening and movements of near-shore landfast ice, and complete clearance of landfast ice off coast, respectively. Melting degree days are defined as

$$\mathrm{MDD}(t) = \int_0^t \begin{cases} \left[T_a(\tau) - 0\ ^\circ\mathrm{C}\right] \mathrm{d}\tau & \text{for } T_a \geq 0\ ^\circ\mathrm{C} \\ \left[0\ ^\circ\mathrm{C}\right] \mathrm{d}\tau & \text{for } T_a < 0\ ^\circ\mathrm{C} \end{cases}, \qquad (1)$$

where T_a is the air temperature at time τ, and t is the time passed since the beginning of the melt season at t=0. In keeping with common practice we express MDD in °C days (i.e., 8.64×10^4 Ks) [Petrich and Eicken, 2010]. However, no models describing summertime break-up have been suggested for the Chukchi Sea coast applicable to Barrow [*George et al.*, 2004].

Other studies have aimed to determine ablation of coastal sea ice and relate ice thickness to summertime break-up. This approach has been motivated by the assumption that thin ice is sufficiently weak to allow dynamic forces of atmosphere and ocean to break up and clear landfast ice off the coast. The role of air temperature as a proxy for the progression of ice decay during spring melt has been investigated by *Bilello* [1980] for various stations mostly in the Canadian Arctic. He found that 120 to 190 melting degree days were required to remove the ice in 8 out of 10 years investigated at Resolute (initial ice thickness 1.9±0.2 m). *Bilello* [1980] also investigated the utility of integrated downwelling shortwave radiation as a proxy for decay. Starting integration on the first day air temperatures exceeded 0 °C, the cumulative shortwave flux ranged between 730 and 1050 MJ/m^2 for the same 8 years at Resolute. However, *Bilello* [1980] did not describe the break-up process at Resolute, leaving it unclear whether ice actually melted in place or drifted out at some point. In recent years, studies of the response of Arctic (coastal) sea ice to climate variability and change included numerical modeling of the seasonal cycle of landfast ice from freeze-up to break-up. While these ice models include the combined effect of snow cover, air temperature and radiative balance, they typically rely on the assumption that dynamic break-up takes place at a date at which the simulated ice thickness decreased to a threshold level, ranging between 0.5 m [*Dumas et al.*, 2006] and 0 m [*Shirasawa et al.*, 2005]. All modeling studies acknowledged the contribution of

dynamic processes to break-up of weakened ice. However, none of the studies focused on the process or definition of break-up itself. Also, the role of disintegrating ice under melt ponds as opposed to ablation of unponded level ice has not been considered explicitly.

We analyzed an 11-year record of break-up observations at Barrow in a location representative of conditions along the Chukchi Sea coast (Figure 1). For the purpose of this study, break-up is defined as the detectable movement of near-shore landfast ice associated with irreversible deterioration and decay of coastal ice in spring (Section 4). In line with past studies [e.g., *Reimnitz et al.*, 1994; *George et al.*, 2004] we consider landfast ice as an aggregate of grounded pressure ridges and attached shoreward level and rubble ice ("near-shore ice", Figure 2). Ice attached seaward of grounded pressure ridges and associated break-out events were considered elsewhere [*Druckenmiller et al.*, 2009] ("attached ice", Figure 2). In years without grounded pressure ridges, that typically help confine near-shore ice, break-up corresponds to final removal of that stretch of ice that remains longest attached to shore at a particular location. The present study aims to characterize the break-up process and investigate its predictability in the context of forecasts on timescales of several weeks.

We derive a data set of break-up times and modes by analyzing ground-based observations recorded by a web camera, a coastal radar and ice observers as well as satellite-remote sensing data to arrive at a better understanding of the landfast ice break-up process at Barrow and examine its variability on the timescale of a decade. While the date of break-up is determined by the coastal topography as well as a range of other factors discussed below [*Mahoney et al.*, 2007a], the landfast ice at Barrow is representative of ice conditions and processes along a wider stretch of coastline in the Alaskan and East Siberian Arctic [*Barry et al.*, 1979; *Druckenmiller et al.*, 2009]. The break-up process will be discussed in the light of available wind, current and tidal data, and thermal decay. Building on the analysis of ice break-up and its interannual variability we then present a simple empirical model to forecast decay and break-up of landfast ice on timescales of days to two weeks. The break-up model is forced by a near realtime long range Alaska weather forecast system (http://knik.iarc.uaf.edu/AtmGroup/ForcastGraphics.htm), which is using the Weather Research and Forecasting (WRF) model [*Skamarock et al.*, 2005] configured for the regional conditions of Arctic Alaska.

2 Ice and ocean at Barrow

We describe a general, simplified picture of ice conditions in the Chukchi Sea with a focus on Barrow, Alaska (Figure 1). The Chukchi Sea coast runs SW to NE from Point

Hope to Point Barrow with the Alaska Coastal Current generally moving to the North-East, with occasional 2 to 10-day periods of current reversal [*Aagaard and Roach*, 1990; *Weingartner et al.*, 1998]. The Barrow Canyon approximately parallels the Chukchi coast about 30 km offshore at Barrow, resulting in a steep bathymetric gradient with the 20 m water depth contour as little as 1 km offshore. The landfast ice edge typically extends out to the 20 to 25 m isobath once a stable landfast ice cover has formed [*Mahoney et al.*, 2007a]. At Barrow and elsewhere along the Chukchi and Beaufort Sea coast, grounded pressure ridges are found at this water depth, helping stabilize the shorefast ice [*Rex*, 1955; *Barry et al.* 1979]. In the Beaufort Sea east of Point Barrow, the 20 m isobath follows the coast in excess of 10 km offshore. Point Barrow presents a small protrusion to the North-West into the Chukchi Sea. While the semidiurnal tidal sealevel variability is less than 0.3 m, the range of sea level variations due to surges can exceed 1 m [*Hume and Schalk*, 1967; *Lynch et al.*, 2008]. In spring and summer, warm waters entering the Chukchi Sea through Bering Strait are steered by bathymetry to follow systematic flow paths [*Weingartner et al.*, 2005; *Woodgate et al.*, 2005]. Most of the variance in currents is explained by local winds [*Johnson* 1989; *Weingartner et al.*, 2005; *Woodgate et al.*, 2005]. Warm waters were observed to contribute most directly to ice melt where they flow perpendicular to the edge of the marginal ice zone and where ice is advected into warm currents [*Paquette and Bourke*, 1981; *Ahlnäs and Garrison*, 1984]. At Barrow, those waters flow approximately parallel to the shore and landfast ice edge in the Alaska Coastal Current [*Weingartner et al.*, 2005].

With the Chukchi Sea generally ice-free during summer in recent years, the ice extent increases from late October to cover the entire Chukchi Sea by late December. While historically landfast ice at Barrow typically started to form during the first week of October [*U.S. Navy Hydrographic Office*, 1958], observations during the recent decade showed landfast ice to form in Barrow no earlier than November [*Gearheard et al.*, 2006]. However, newly formed landfast ice is prone to breaking out during storms, resulting in years of landfast ice formation as late as mid-December (e.g. 2006 and 2007, and presumably some years between the 1930s and 1950s [*U.S. Navy Hydrographic Office*, 1958]). Landfast ice present in late December will remain in place until break-up in summer.

Usually ice conditions in winter are conducive to the formation of grounded pressure ridges between 500 m and 2 km off the Barrow coast with sail heights in excess of 3 m. The sheltered near-shore zone between grounded pressure ridges and shore is filled with pack ice, formerly landfast sea ice that drifted in from elsewhere, and ice that grew in place [cf. *Shapiro and Barnes*, 1991]. This conglomerate of near-shore ice can be divided

into 100 m to km-size patches of either deformed, rubble ice (surface ice profile variation in excess of 0.2 m) or level ice (i.e., surface profile variations are not apparent without dedicated measurements).

Our measurements at Barrow [*Druckenmiller et al.*, 2009] show that ice thickness of level near-shore ice increases from 0.6 to 0.8 m in January to reach its maximum of 1.4 to 1.6 m in mid May. The mean snow depth on near-shore ice can be less than 0.1 m in early January. Snow dune depth may exceed 0.3 m in early May. Snow melt begins in May and patches of bare ice and melt ponds appear in early June. Melt pond formation is generally first observed offshore of downtown Barrow in May where snow is often visually dust-covered, and progresses northward over the following days or weeks until it reaches UIC-NARL and Point Barrow in the first half of June. Due to their low albedo compared to bare or snow-covered sea ice [*Grenfell and Perovich*, 2004], melt ponds greatly enhance surface ablation and internal melt of sea ice. The typical length scale of snow dunes and melt ponds is 5 to 15 m (cf. insert in Figure 3). Barrow experiences perpetual daylight from 11 May until 1 August. In addition to surface ablation, decreased sea-ice surface albedo and a reduction of ice concentration in the Chukchi Sea allow increased solar heating of the ocean, contributing to ice decay by increasing the porosity of sea ice and promoting bottom melt of level ice and pressure ridges (Figure 2).

3 Methods

3.1 Ice

The sea ice melt season has been recorded by a webcam positioned at various locations between downtown Barrow and the research support center at the Ukpeagvik Iñupiat Corporation Naval Arctic Research Lab (UIC-NARL) since 2000. The webcam overlooked shore, ice and sky at UIC-NARL during the summers 2000 to 2005 (2000–3: 71.33˚N 156.68˚W, 10 m above ground; 2004–5: 71.33ºN, 156.67ºW, 8 m above ground, facing WNW) and at downtown Barrow since the melt season 2006 (71.29º N, 156.79ºW, 23 m above ground, facing NNW). Images were recorded every 5 minutes. Ridged and rubble ice features and summer melt ponds can be discerned, allowing detection of ice motion. Image contrast is too low to discern features on days of low visibility, i.e., on a few days in June and July. The best overview of ice conditions off UIC-NARL was obtained 2000–3.

Scattering of radar signals off sea ice surface features provides distinct return signals that are used to track sea ice motion. A Raymarine X-band 10 kW radar (10 GHz, 3 cm), recording one image every 5 minutes was placed at UIC-NARL in the summers of 2004

and 2005, i.e. within the footprint of earlier radar observations [*Sackinger and Rogers*, 1974; *Shapiro and Barnes*, 1991]. In 2006, a Furuno 12 kW X-Band radar was permanently installed next to the webcam in downtown Barrow. At a range of 10 km data from the radar downtown extend past UIC-NARL and provide spatial continuity for break-up observations. Webcam, radar, and routine ice observations are part of the Barrow coastal observatory and accessible online (http://seaice.alaska.edu/gi/) [*Druckenmiller et al.*, 2009].

To supplement the coastal observations in spring and summer we used satellite images, primarily from the optical systems Moderate Resolution Imaging Spectrometer (MODIS, onboard satellites Aqua and Terra) and Landsat. Reprojected Landsat images were obtained through the USGS Global Visualization Viewer, while reprojected MODIS images since 2004 were provided by the NASA MODIS Rapid Response System. In addition, we reprojected Level 1B MODIS images from 2000 to 2003 with the USGS MODIS Reprojection Tool – Swath. Although visible satellite images are subject to clouds, we obtained valuable information to supplement the radar and webcam observations due to generally light cloud coverage in Barrow in June and July, and a comparatively high rate of overpasses of Aqua and Terra satellites, providing a combined 8 to 12 potentially usable overpasses daily. RADARSAT and European Remote Sensing Satellite (ERS-2) Synthetic Aperture Radar (SAR) images to complement the analysis were provided by the Barrow Area Information Database (BAID) project.

3.2 Ocean

Near-shore oceanographic measurements are available at Barrow during two years of the investigated period. From August 2008 until August 2010, the National Oceanic and Atmospheric Administration (NOAA) operated moorings 3.5 km North-West of UIC-NARL (station 9494935, 71.36˚N, 156.73˚W), recording sealevel data with pressure transducers every 6 minutes (Figure 1). In addition, we deployed a near-shore oceanographic mooring with Teledyne Sentinel WH-300 Acoustic Doppler Current Profiler (ADCP) approximately 36 m beneath the sea surface, and Sea Bird Electronics SBE 37 and 39 instruments as part of the coastal observatory from August 2009 until August 2010. Velocity data were recorded in 2 m vertical intervals every 15 minutes. The mooring, referred to as *B1*, was located 7 km west of UIC-NARL at a water depth of 42 m (71.325˚N, 156.884˚W, Figure 1). Data are available through the Cooperative Arctic Data and Information Service of the Arctic Observing Network (http://aoncadis.org).

3.3 Atmosphere

3.3.1 Observed irradiance

Downwelling broadband irradiation measurements are available through the Department of Energy Atmospheric Radiation Measurement (ARM) program starting in 2000. Automated measurements performed North-East of UIC-NARL on tundra and are generally available with 3 to 5 day delay. ARM data are the reference irradiance in this study, and the latest data available are used during the break-up forecast.

3.3.2 Weather station data

We use hourly aviation routine weather reports (METAR) of the Barrow airport (PABR) to obtain a historical record of air temperature, wind speed and direction, and historical and up-to-date information on both cloud cover, respective ceiling height and runway visibility to estimate downwelling shortwave flux. The airport is located near downtown (71.29˚N, 156.76˚W). For break-up forecasts, we bridge the temporal gap between ARM data and forecasts with irradiance estimates based on the METAR record. The method of estimating downwelling shortwave radiation based on cloud, visibility and day of year is described in Appendix B.

3.3.3 Weather forecast

The atmospheric forcing for the break-up forecast is the hourly output at Barrow from the 16-day long range Alaska weather forecasts. The forecasts are produced by the Weather Research and Forecasting (WRF) model in which the initial and boundary conditions are driven by the 16-day extended forecasts of the Global Forecast System (GFS) operated by the National Centers for Environmental Prediction (NCEP). The WRF forecast domain is centered over the Seward Peninsula, Alaska on the polar stereographic projection and is bounded by latitudes 50º N and 80º N, by the New Siberian Islands and by Banks Island. The horizontal resolution of the forecast domain is 20 km.

The Alaska WRF forecast system is configured with model physics of the Goddard shortwave [*Chou and Suarez*, 1994] and the Rapid Radiative Transfer Model (RRTM) longwave [*Mlawer et al.*, 1997] for the radiation transfer calculations, and the land surface model NOAH [*Chen and Dudhia*, 2001] for surface physical processes, in which the surface albedo of 0.65 is used for a grid cell covered by sea ice. Ice coverage (either 0% or 100%) and sea surface temperature are prescribed by the GFS forecasts.

Our investigations with ARM irradiance measurements show that the WRF forecasted downwelling shorwave irradiance is biased. In order to improve the irradiance forecast we apply an empirical correction, which is outlined in Appendix B.

4 Results

4.1 Break-up process

A description of the break-up process of landfast ice at Barrow from summer 2000 to summer 2010 is provided in Appendix A. Here, we summarize these observations through specific examples. Observations show that two fundamental modes can be discerned. In years with grounded pressure ridges the near-shore ice decays in place (surface water visible between pieces of white ice in Figure 4a) until winds and currents are able to move it along the coast while pressure ridges remain in place (as seen in Figure 4b showing a different configuration of near-shore ice while pressure ridges are still in place). Over the course of days or weeks after the initial dislocation and movement of near-shore ice (Figure 4c), pressure ridges break out or melt in place (Figure 4d). Based on interpretation of webcam images, no evidence of fracturing of islands of unponded level ice at break-up could be observed, suggesting that ice beneath melt ponds had either melted completely or weakened to fail and allow for drift under moderate forces. Since the controlling factor in the break-up process is the melt of ice under meltponds we refer to this mode of break-up as *thermal break-up*. The other fundamental mode appears in years of few or absent grounded pressure ridges that allow weaker dynamic forces to trigger break-up. In this case ice has weakened and the near-shore ice and pressure ridges fracture under the influence of mechanical forces, breaking out simultaneously during weather events and clearing the shore within hours. Hence, we refer to this break-up mode as *mechanical break-up*.

For consistency we define break-up as the first day on which movement of ice near-shore is detected at UIC-NARL. Break-up happens generally earlier in years of mechanical break-up than in years of thermal break-up (cf. Table 1; Appendix A). While break-up is defined based on point observations, the process can be placed into broader context with the help of satellite images. As an example of thermal break-up, consider the sequence of events illustrated in Figure 5 showing MODIS imagery for 2006. The defining feature is the persistence of pressure ridges off-shore extending tens of kilometers south of Barrow (not shown) while near-shore ice melts and moves alongshore, and the presence of an ice plug north of Point Barrow preventing flushing of near-shore ice to the North. First signs of complete melt offshore of downtown Barrow appear on 3 July. Near-shore ice moved south at UIC-NARL on 6 July as recorded by the coastal radar. Disintegration continued

north of UIC-NARL, with drift past Point Barrow possible after 11 July. A clear passage past Point Barrow was open on 22 July, while grounded pressure ridges were still in place offshore 2 weeks later on 4 August. The coast was ice-free on 9 August. The stability and the protecting effect of grounded pressure ridges can be observed between 11 and 22 July when pack ice moves in and closes the coastal lead while the region shoreward of the pressure ridges remains ice-free.

A case of thermal break-up in an ice year more typical for the last 11 years is illustrated in Figure 6 for the year 2008. That year, the defining feature was the development of an open passage for ice drift to the North at about the same time as near-shore ice became mobile. Once the ice had been weakened in place, it was flushed out of the coastal zone to the North. Landfast ice north of Point Barrow was dislodged between 30 June and 5 July. First signs of open water were present at the shore on 7 July with signs of near-shore ice redistribution by 8 July. A clear passage for near-shore ice to drift north past Point Barrow existed from 9 July onwards. The flaw lead lining the outer landfast ice edge opened and pack ice retreated 13 July, leaving grounded pressure ridges behind. Remaining ice drifted off on 23 and 24 July. The complexity of ice drift patterns at the time of break-up is not apparent from MODIS imagery. For example, while the coastal radar recorded motion to the north-east in the coastal lead from 3 to 17 July, near-shore ice south of UIC-NARL moved along the shore to the south-west to enter the lead between Barrow and Browerville (Figure 1) on 7 June and on several occasions thereafter.

Figure 7 illustrates mechanical break-up in 2007. The defining features are ice breaking out successively along the coast south to north without preceding near-shore ice movement. The lead was open with landfast ice in place on 20 June. Some ice was lost south of Barrow and along the lead edge by 25 June (see also Figure 3). All landfast ice was broken out by 28 June, with only one ice island still grounded off-shore of Barrow. Not shown is a RADARSAT image of 26 June revealing that landfast ice was still in place that day. Mechanical break-up in the form of ice breaking out at UIC-NARL occurred on 27 June, documented by coastal radar.

Break-up dates and the period of disappearance of pressure ridges at UIC-NARL are summarized in Table 1 and shown in Figure 8 (Appendix A). We classify break-up in 2003, 2004, 2007, and 2010 as mechanical, and all other years, except 2002, as thermal. 2002 remains unclassified because both ice formation and break-up processes were unusual. In 2002, grounded pressure ridges did not form until March, with the water between the coastal shorefast ice and pressure ridges freezing afterwards. In this case we

consider break-up as the movement of the original shorefast ice rather than the earlier (7 June) movement of the thinner ice that formed since March. In addition to differences in landfast ice formation, surface melt may have progressed differently in 2002 compared to other years investigated. Using ARM data of tundra albedo as a proxy, in 2002 snow melt and meltpond formation proceeded in a two-stage evolution, first significantly advancing around 25 May, but then being temporarily stalled by a cold spell and overcast conditions until early June.

4.2 Dynamic forcing

Throughout the year, winds at Barrow come predominantly from easterly directions between 5 and 10 m/s (10 to 20 knots) (Figure 9a). Wind speeds on days of break-up were typically around 5 to 7 m/s (Figure 10), i.e., within the range of commonly observed wind speeds at Barrow, with the strongest winds of approximately 10 m/s observed in 2003, 2005, and 2007. Winds were observed to come from any direction during break-up, except from south and south-east (Figure 10). In 6 out of 11 years, winds came from westerly directions (2001, ‘02, ‘04, ‘05, ‘09, ‘10), while winds blow from westerly directions less than 25% of the time in June and July (Figure 9b). This difference is statistically significant at the p=0.05 level. The direction of ice drift during thermal break-up was recorded by webcam and coastal radar. Near-shore ice drifted to the south-west in years with winds from either easterly (2000, ‘06) or westerly directions (2001, ‘02, ‘09). Drift to the north-east was only observed in two years. In 2005, winds blew from westerly directions, while in 2008 the wind direction changed from east to north-west at the time of break-up. While ice motion during the general break-up period in 2008 was complicated (see above), in all years for which we have radar observations of drift in the coastal lead during thermal break-up, ice in the coastal lead and near-shore ice at UIC-NARL drifted predominantly in the same direction (2006, ‘08, ‘09).

In 2010, data are available on currents and sealevel near UIC-NARL. Measurements during the break-up period are shown in Figure 11 with break-up and notable break-out events before and after break-up highlighted (cf. Appendix A). Ocean temperatures during break-up period ranged between -2 and 6 °C at 36 m depth, and currents more that 2 m below the sea surface were moving to the North-East with the exception of the two days preceding a break-out event at downtown Barrow on 25 June (cf. Figure 12). Notably, the brief period with currents to the South-West was associated with water temperatures decreasing to the freezing point, while currents to the North-East were associated with temperatures rising. A notable change in wind direction from south-west to north occurred during break-up on 4 July. Sea surface level variation was small with the highest sea level recorded following 8 July and lasting during the break-out event

dislodging grounded ridges on 9 July. Also, both sustained wind speeds and near-surface currents peaked at 10 m/s and 1.1 m/s (Cell 15 in Figure 11), respectively, at the end of 8 July.

4.3 Ice decay

Figure 13 shows the accumulation of melting degree days until break-up with the final values listed in Table 1. By the date of thermal break-up, approximately 110 to 120 melting degree days have accumulated, with the exception of 2001 and 2005, where thermal break-up occurred at between 60 and 80 melting degree days. Years of mechanical break-up experienced the complete removal of all ice at UIC-NARL after 30 to 70 melting degree days.

Figure 14 shows the cumulative irradiance at the time of break-up for different start dates of integration. While the cumulative irradiance decreases as the start of integration approaches the date of break-up, it is noticeable that the years of thermal break-up and 2010 are closely clustered compared to the remaining years. For years of thermal break-up the range of cumulative irradiance is lowest for start days around day 158. As an example, we consider a start date of 5 June, i.e. the date used for the break-up forecast. Based on a start date of 5 June, years of thermal break-up accumulated between 700 and 760 MJ/m^2, while years of mechanical break-up and 2002 experienced break-up after 560 to 590 MJ/m^2, with the exception of 2010 in which 700 MJ/m^2 were accumulated (Table 1). The irradiance trajectories are shown as a diagram of cumulative irradiance versus average irradiance in Figure 15. Comparing average irradiance early in the melt season with average irradiance at break-up we notice that some years show little correspondence (2000, ‘05, ‘06) while other years are consistently low (2009) or high (2004, ‘07). At the time of break-up, the average irradiance was highest in the four years of mechanical break-up (2003, ‘04, ‘07, ‘10).

4.4 Forecast

Using the cumulative irradiance as an indicator for thermal break-up, we operated a break-up forecast during the melt seasons 2009 and 2010 (presented in the Study of Environmental Arctic Change (SEARCH) Regional Sea Ice Outlook; www.arcus.org/search/seaiceoutlook). Break-up was forecast to take place as soon as a threshold cumulative irradiance was reached. Figure 16 shows the range of error in the break-up prediction for different start dates of integration. The calculations are performed in hindsight, i.e. based on actual ARM irradiance measurements rather than irradiance forecasts. For each start day in this figure, the cumulative irradiance threshold for break-up was chosen to be the lowest cumulative irradiance observed at break-up. The best

performance would have been obtained for a starting day-of-year 158, i.e. 7 June (cumulative irradiance threshold 655 MJ m^{-2}).However, we performed the operational break-up forecast based on a start date of 5 June for consistency with past predictions. Operating the break-up forecast with both measurements and irradiance predictions, Figure 17 illustrates the history of predicted break-up dates for the 2009 season, a year of thermal break-up. Until 26 June, the break-up forecast was indicating that break-up was expected outside the range of the weather forecast. From 26 June on, the break-up forecast was consistent to within one day and eventually fell on the exact date of observed break-up. Break-up in 2010 was classified as mechanical break-up and is thus outside of the range of applicability of the forecast. However, the 2010 break-up forecast was consistent to within two days since 20 June (not shown), and the predicted date was off by one day.

5 Discussion

5.1 Break-up process

Our observations show that landfast ice break-up at Barrow is a two-stage process where thermal decay of near-shore ice is followed by dynamic forces that cause the near-shore ice to dislodge, defining break-up. In years without grounded ice offshore (mechanical break-up), the landfast ice weakens from heat supplied by ocean and atmosphere. In response to dynamic forces, large chunks break off and disperse into the Chukchi Sea. In years with grounded ice offshore (thermal break-up), the near-shore ice is exposed to heat supplied by ocean and atmosphere for a longer period of time, leading to the most significant decay in ice under melt ponds. With significant decay under melt ponds, the adjacent stretches of level unponded ice are eventually advected parallel to the coast in response to dynamic forces. Once this ice is mobilized, the grounded ice breaks out as it continues to melt. The dynamic forces that trigger break-up could be either of a sporadic nature like a swell that overwhelms ice stability, or continuously present, eventually outgrowing ice strength as the ice weakens. Candidates for thermal decay of the ice are heat flux from ocean and atmosphere, surface meltwater, and radiation balance.

In all years of mechanical break-up, the average irradiance at break-up was comparatively high. Hence, there is some indication that, in addition to cumulative irradiance, higher mean irradiance may be conducive to mechanical break-up as it aids decay and ungrounding of stabilizing ridges [*Mahoney et al.*, 2007b] and level ice. Barring knowledge of the grounding and stability of landfast ice, the irradiance trajectory of a given melt season (Figure 15) may serve as an indication of the likelihood of mechanical break-up.

5.2 Dynamic forcing

We found that break-up is not associated with unusually strong winds. However, amongst the three years of highest wind speed during break-up were both mechanical break-up events that happened during easterly winds (2003, ‘07). Hence, strong easterly winds (i.e. offshore winds) may be conducive to mechanical break-up.

With the disproportional likelihood of observing westerly winds during break-up, wind fetch across the Chukchi Sea and resulting waves, swell, elevated sealevel, and storm surges are candidate forces for break-up. While we have no measurements of waves and swell, wave action is known to be able to fracture ice in the marginal ice zone and landfast sea ice [*Fox and Squire*, 1991; *Langhorne et al.*, 1998; *Squire*, 2007]. Elevated sealevel was not observed during break-up in years we have data for (2009, ‘10). However, following break-up in 2010, sealevel was observed to be slightly elevated during a break-out event of grounded pressure ridges during easterly winds. This indicates the possibility that sealevel changes may help dislodge grounded ice, which could facilitate mechanical break-up in years with only weakly grounded ridges.

During thermal break-up, winds came from either easterly or westerly directions without a clear correlation between winds and ice drift. This lack of correlation is not surprising considering that radar observations of ice drift show that the potential influence of currents and winds on drift is of the same order of magnitude. Observed break-up could be delayed with respect to the stage of decay if motion is restricted in the direction of dynamic forces. However, melt in the near-shore region (e.g., 2006) and drift through passages in the discontinuous line of pressure ridges (e.g., 2008) do take place and reduce the practical importance of any restriction to the North-East or South-West of UIC-NARL. Winds were not observed to come from the South and South-East during break-up, which is consistent with the general absence of winds from that direction.

5.3 Ice decay

There is agreement in magnitude between the range of accumulated melting degree days observed in years of thermal break-up at Barrow (i.e., 60 to 120 melting degree days) and the range reported by *Barry et al.* [1979] for the onset of ice movement in the Beaufort Sea (i.e., 55 to 140 melting degree days). The range reported by *Bilello* [1980] for the complete removal of ice at Resolute was higher (120 to 190 melting degree days), similar to the respective range reported by Barry et al. [1979]. In addition, the cumulative irradiance at break-up reported by *Bilello* [1980] (730 to 1050 MJ/m^2) is of the same order of magnitude we found for thermal break-up (700 to 760 MJ/m^2). Had we chosen a start date of integration based on air temperature above 0 °C, our values would have been

higher. For example, we see from Figure 14 that a start day around 145 would have brought us into the same range as *Bilello* [1980], including both mechanical and thermal break-up events. Warm spells with partial snow melt are common in Barrow around day 145 (25 May), leading us to conclude that irradiance observed by *Bilello* [1980] at Resolute is consistent with our observations at Barrow.

Since sea ice temperature in the melt season is nearly isothermal [*Petrich and Eicken*, 2010], the conductive heat flux through the ice is small and the turbulent atmospheric heat flux and the oceanic heat flux will mostly contribute to surface and bottom ablation, respectively, weakening the ice by reducing thickness. Irradiance is absorbed both near the surface and in the ice interior, contributing to decay and loss of strength by increasing porosity. For example, ice of 1.5 m thickness with porosity 0.9 and albedo 0.4 (melt ponds) would be completely melted by absorbing 690 MJ/m^2, a magnitude that could be realistically reached by the time of thermal break-up. Hence, we expect that ice under melt ponds has most likely melted by the time of thermal break-up. The potential contribution from turbulent atmospheric heat flux is smaller. In order to melt the example ice, assuming a surface temperature of 0 °C and an ice–atmosphere heat transfer coefficient of 10 $Wm^{-2}K^{-1}$, 480 melting degrees would be necessary, vastly exceeding the 80 and 62 melting degree days observed in 2001 and 2005, respectively. Hence, irradiance is the single most important contributor to decay leading to thermal break-up. However, considering mechanical break-up, average strength of landfast ice is more important and therefore ice thickness and melting degree days will have higher skill as indicators for the state of decay.

5.4 Forecast

Past approaches to predicting coastal ice break-up have mostly relied on melting-degree modeling as a measure of the total amount of heat supplied to melt ice, thereby structurally weakening and priming it for break-up [*Bilello*, 1980; *Gudkovich*, 1995]. Russian scientists have also developed empirical or statistical models that take into consideration wind speed and the local topography in predicting break-up dates [*Gudkovich*, 1995]. Based on melting degree days in Figure 13, we find that a threshold of 110 °C-days could be used as an indicator for break-up in 2000, 2006, 2008, and 2009. However, thermal break-up in 2001 and 2005, break-up in 2002 and mechanical break-up cannot be explained by this threshold alone. Also, the observed range of 60 to 120 melting degree days is too broad to be useful for forecasts, translating into the equivalent of approximately 10 to 14 days of uncertainty.

Given the prominent role that solar heating plays in ice decay [e.g., *Perovich and Maykut*, 1990], the spatial heterogeneity of a melting Arctic sea ice surface, and considering spatial heterogeneities in the surface air temperature field in coastal regions, the aforementioned spread in melting degree days is to be expected. Here, we took an approach employed in numerical sea ice models and advanced statistical models of glacier ablation by integrating measures of irradiance [*Hock*, 1999]. Data from Barrow indicate that thermal break-up occurred once a threshold in the cumulative irradiance recorded at the ARM site had been passed (700 MJ/m^2, starting integration at 5 June, cf. Figure 15). This relationship allowed for prediction of break-up in all years of thermal break-up. While the start date for the integration of shortwave flux was empirically set to 5 June, a time during which melt ponds are observed to proliferate along the coast of Barrow, the choice of start date is not critical if the threshold is adjusted accordingly.

We chose to operate the forecast with a fixed start date for all years, unlike the investigation by *Bilello* [1980] that started integration on the first day of temperatures above 0 °C. At least at Barrow, both choices are arbitrary. Brief periods of temperatures above 0 °C were observed as early as April (e.g., 2002, ‘03, ‘04, ‘05, ‘09), at a time of ice growth and increase in snow depth and clearly before the onset of appreciable melt. While temperatures above 0 °C recorded at the Barrow airport have been associated with snow melt on the tundra [*Stone et al.*, 2002], there is currently no evidence of a correlation with meltpond development. Further, onset of meltpond development is a gradual process at Barrow, propagating South to North over the course of days to weeks. Hence, we chose to use a fixed date.

There is a degree of uncertainty in the forecast procedure as little account is taken for the initial ice conditions [cf. *Gudkovich*, 1995]. While ice thickness in May has been relatively constant throughout the years, we only consider the difference between grounded landfast ice (leading to thermal break-up) and ungrounded landfast ice (leading to mechanical break-up). Inter-annual variability of the degree of deformation and sediment entrained in the ice are not accounted for, both of which should affect absorption of light and meltpond development. Also, variability of snow depth and the timing of meltpond development are assumed invariants.

Considering only decay in the forecast we made an implicit assumption about dynamic forces. Decay is a continuous process while dynamic forces may either be continuous (e.g., winds, currents) or transient (e.g., winds, currents, swell, waves, tides, gusts). In the present break-up forecast we assumed that dynamic forces apply continuously. However, at least in 2008 when thermal break-up occurred at a time of changing wind direction,

transient forces may have been important. The inclusion of dynamic forces into the prediction of break-up should improve forecast skill.

While two years is too short a time to reach definite conclusions about the skill of forecasts of springtime irradiance, the consistency in forecast break-up dates (Figure 17) suggests that systematic correlations might exist between forecast and observations at the comparatively long time scale of two weeks.

5.5 Definitions of landfast ice break-up

We focused on one particular definition of break-up in the previous sections, based on a physical process at one reference location in the previous section. However, break-up has been defined differently to accommodate specific operational considerations or data limitations [e.g. *Kniskern and Potocsky*, 1965; *Mahoney et al.* 2007a].

An alternative definition may be based on observed community access to the sea from the Chukchi Sea coast. Independent of this study, records of Barrow community members are available on the first day of boating activity launched from the Chukchi Sea shore [*C. George*, personal communication, 2010]. The boating records shown in Figure 8 indicate that the break-up process defined here in purely physical terms is associated with one of the key activities in the local community, access to the sea from the beach. In general, boating activity is observed around the same time as movement of near-shore ice. In years where boat access leads break-up at UIC-NARL, coastal ice broke up in stages from the South (near the residential areas of Barrow) to the North (at the reference point of this study). This is in particular the case for 2009 and 2010 where earlier break-up was observed right at downtown Barrow (Figure 12). In contrast, the comparatively delayed start of boating activity in 2006 resulted from a pronounced line of grounded pressure ridges that limited the possibilities for dispersal of disintegrating near-shore ice and boat access further offshore (Figure 5).

Differences in the dates of break-up and boating presented here may serve to illustrate that stages of the sea ice cycle are defined in relation to a specific purpose or use of the ice cover [*Eicken et al.*, 2009]. While break-up in this study was defined to systematically investigate a physical process, this definition only approximates the requirements of boat access. Yet, within the limits discussed above, the consistently acquired set of physical observations can be used as indicator for conditions that are meaningful in a broader context.

5.6 Historical accounts

Sackinger and Rogers [1974] and *Shapiro and Barnes* [1991] documented break-up at UIC-NARL in the 1970s based on imagery from a coastal X-band radar. Their description mirrors our observations of 2006, with the largest ridge tracing the 20 m-contour. They reported disintegration of the line of pressure ridges once the near-shore ice fractured into small floes and started to move. According to the detailed account of *Sackinger and Rogers* [1974] on ice break-up in 1973, near-shore ice did not start to move significantly until 22 July 1973, with pressure ridges completely drifted out on 3 August. By our definition, this break-up appears to have happened 11 days later than the latest break-up observed since the summer of 2000 (Table 1). The break-up process reported for the 1970s is consistent with thermal break-up, with the exception of the heavy ice year 1975 in which landfast ice remained along the shore throughout summer [*Shapiro and Barnes*, 1991].

Our observations can be placed in historical context based on observations of the *U.S. Navy Hydrographic Office* [1958]. Here, break-up is defined as the date the ice concentration decreases to 10% [*Kniskern and Potocsky*, 1965], which is similar to our record of the break-out of pressure ridges (Table 1). Based on a summary of 25 (unspecified) years of observation starting in the 1930s, according to their definition, break-up at Point Barrow happened at the earliest and latest on 15 June and 24 August, respectively, with an average given as 24 July [*Kniskern and Potocsky*, 1965]. Range and average compare well with the times of the disappearance of pressure ridges in Table 1, suggesting that both thermal and mechanical break-up used to occur at Barrow 50 to 80 years ago. However, noting that a typical time for the disappearance of pressure ridges would be around 15 July in our case (Table 1), it appears that grounded pressure ridges, when they formed, used to be either better anchored than they generally have been since 2000, or better protected from ocean swell by pack ice in the Chukchi Sea [*U.S. Navy Hydrographic Office*, 1958]. Ice conditions observed in 2006 are likely typical of this more traditional ice regime, as also noted by local ice experts [*R. Glenn*, personal communication, 2006].

6 Summary and Conclusion

In this work we took the long-recognized and often repeated concept “break-up=ice decay+dynamic forces” literal and attempted to separate the decay process from the dynamic process. The novel aspect of this work is the combination of an in-depth investigation of the break-up process, previously limited to studies of one season, with an investigation of the predictability of break-up, which is limited to long-term studies. As a

result, this appears to be one of the first studies of the inter-annual variability of the break-up *process* of landfast sea ice. Key insights gained include the value of discriminating two almost consecutive modes of decay of landfast ice (general weakening of the ice cover vs. almost complete disintegration of ice under meltponds), and the contribution of inter-annual variability of ice conditions (spatial confinement due to grounded ice) on the mode of decay relevant during break-up. While previous studies often considered break-up at multiple locations, the transferability of our results will still have to be tested. However, considering that both melting degree days and cumulative irradiance at break-up reported throughout the Alaskan and Canadian Arctic agree with our observations at Barrow, and considering that embayments may be sheltering landfast ice similarly to grounded ridges, our results are likely transferable. For example, investigating which of the two ice decay modes dominates at a particular location may guide the selection of indicators for break-up forecasts in the Canadian Arctic and elsewhere, e.g. leading to the use of predominantly dynamic indicators in exposed areas and thermodynamic indicators in sheltered areas. Also, regions with low forecasting skill may turn out to exhibit a bi-modal distribution of break-up modes similar to Barrow, a potentially helpful insight for forecasting. The suggested distinction between two break-up modes applies to ice forming meltponds, i.e., Arctic sea ice.

We compared environmental conditions leading to break-up at Barrow from 2000 to 2010. While the reduction of ice thickness and internal weakening are important decay mechanisms for mechanical break-up, thermal break-up was preconditioned by the decay of ice under meltponds. Break-up was observed disproportionally often during onshore (westerly) winds, leading us to suggest that oceanic forces like waves or swell may have contributed to break-up. Offshore (easterly) winds seemed to have to be strong for mechanical break-up to occur, indicating the importance of atmospheric forces. We found no evidence that strong currents or high tides are necessary for break-up during a rare coincident measurement of oceanic currents in 2010. Current reversal and speeds as high as 1 m/s were observed during separate break-out events a few days before and after break-up, respectively. The oceanographic measurements also show the increasing heat content of nearshore waters as a result of solar and possibly advective heating, both promoting thermal decay and break-up.

This work highlights the importance of grounded pressure ridges for the stability of landfast sea ice in the Alaska Arctic, and the significant inter-annual variability of break-up dates observed during the past decade. Further, the study adds evidence to the fundamental importance of meltponds in the break-up process. The near-shore environment allowed us to observe the transition from the commonly acknowledged

preferential melt of melt ponds on a single piece of ice to agglomerates of ice floes with significantly larger cumulative perimeter, marking the beginning of a non-linear, catastrophic disintegration of landfast ice driven by both lateral, top and bottom ablation.

We have identified two physically distinct modes of break-up of landfast ice at Barrow over the past eleven years. Six years of thermal break-up were characterized by significant melt in the near-shore zone in the presence of stabilizing pressure ridges, while in four years of mechanical break-up the landfast ice broke out in large pans with ice in less advanced stages of decay. One year (2002) exhibited characteristics of both thermal and mechanical break-up. Based on historical data, we inferred that both modes likely occurred between the 1930s and 1950s, and that break-up between 1973 and 1976 was likely thermal every year. While neither break-up mode is unheard of, we may add from eye witness accounts of Barrow hunters that the prevalence of mechanical break-up in the recent decade is unusual on a 30-year time scale.

We have compared two empirical measures for break-up progress, melting degree days and cumulative irradiance, and found cumulative irradiance to be the more precise indicator for thermal break-up of landfast sea ice at Barrow. The observed range in melting degree days until break-up at Barrow matches previous reports for the Beaufort Sea coast, leading us to conclude that the irradiance approach may be transferable along the Beaufort Sea coast and possibly also along the east coast of the Chukchi Sea.

Based on two years of break-up forecasts, it appears that the timing of thermal break-up can be gauged two weeks in advance on a 3-tiered scale of “early”, “average” and “late”. Future work on timing and variability of landfast ice break-up should record the break-up mode to guide the development of location-specific ice forecasts.

Acknowledgements

This work was funded by the National Science Foundation (NSF) Seasonal Ice Observing Network (SIZONET), award #OPP-0856867. The break-up forecast was operated in 2010 through an award to CP of the Alaska Center for Climate Assessment and Policy (ACCAP). Satellite images of the Advanced Land Observation Satellite (ALOS) were acquired under an International Polar Year (IPY) award of the Alaska Satellite Facility (ASF) to CP. We appreciate Richard K. Glenn and Dr. J. Craig George sharing observations on ice conditions and community activities with us. Dr. Daisuke Simizu and Dr. Katsushi Iwamoto contributed to the oceanographic measurements. Rachel Potter provided comments on Chukchi Sea oceanography. The use of freely available data sets is gratefully acknowledged: irradiance data of the Department of Energy Atmospheric Radiation Measurement (ARM) program, airport weather data and weather forecasts of the National Oceanic and Atmospheric Administration (NOAA), satellite data of the National Aeronautics and Space Administration (NASA). Additional data portals used for this project were operated by the Geographic Information Network of Alaska (GINA), and the Barrow Area Information Database Internet Map Server (BAID-IMS). The computational support for the realtime Alaska WRF weather forecast was provided by the Arctic Regional Supercomputing Center (ARSC) at the University of Alaska Fairbanks. This study was motivated by and devised as a contribution to the Study of Environmental and Arctic Change (SEARCH) Sea Ice Outlook and we appreciate the support by the National Science Foundation and the SEARCH Project Office at the Arctic Research Consortium of the U.S. (ARCUS) that helped sustain the Outlook. The constructive comments of two anonymous reviewers helped to improve the manuscript.

Appendix A

Below follows a description of the break-up process at UIC-NARL, 5 km NE of Barrow, Alaska, for the years 2000-2010. Descriptions are based on data from web cam (w/c), Landsat (L/S), AVNIR-2 (A) or MODIS (M) imagery, RADARSAT (R/S) or ERS-2 (E), and coastal radar (c/r).

2000: Thermal break-up on 10 July

Near-shore ice moved briefly during three discrete events prior to break-up. An ice shove took place on 26 June (w/c), and slight, momentary southbound movement of ice close to the shore was observed on both 2 July and 5 July (w/c). Starting 10 July, near-shore ice movement was continuously southbound (w/c), defining break-up. The line of pressure ridges started to disintegrate both north and south of UIC-NARL between 14 July and 21 July (L/S, M). They were present at UIC-NARL until they disappeared at an undetermined point in time between 28 July and 31 July (w/c). Break-up happened during winds of 10 to 15 knots from NE.

2001: Thermal break-up on 5 July

Apart from an ice shove on 19 June (w/c), landfast ice was stationary until near-shore ice started to move south on 5 July (w/c). The remaining ice moved out on 7 July (w/c). Break-up happened during 10 knot winds from NW.

2002: Break-up on 30 June

Undeformed landfast ice remained in place without being stabilized by pressure ridges throughout winter, showing the same extent on 19 March, 2002 as it did on 21 October, 2001 (w/c). Grounded pressure ridges formed in March offshore and detached from this ice, allowing the open water between pressure ridges and landfast ice to freeze. This young landfast ice was presumably blown out between 4 June and 7 June (w/c). Until 19 June, the Chukchi Sea lead opened and closed several times seaward of the pressure ridges. Ice was observed to drift southbound through the space between near-shore ice and pressure ridges on 15 June (w/c). Further, the line of pressure ridges started to disintegrate from 18 June (w/c). Chukchi Sea ice pushed toward the shore past the remaining grounded ridges up to the near-shore ice on 19 June (w/c). In this configuration, surface melt of the near-shore ice progressed and the near-shore ice began to drift South on 30 June (w/c). The coastal lead opened on 10 July, followed by the disappearance and melt of remaining pressure ridges by 16 July (w/c). Based on ARM data, 2002 exhibited a significant reduction of tundra albedo by 25 May, one to two weeks earlier than in other years since 2000. Hence, large-scale surface melt, including

melt on sea ice, may have followed an usual trajectory in 2002. Break-up happened on 30 June when winds sustained 15 knots from W.

2003: Mechanical break-up on 25 June

After a large chunk of landfast ice broke out South of UIC-NARL on June 24 (M), seaward deformed landfast ice broke out on 24 June (w/c) (break-up), followed by the remaining near-shore level ice on 25 June (w/c). Break-up happened during 10 to 15 knot winds from E.

2004: Mechanical break-up on 18 June

Coastal ice from several km North of UIC-NARL to several km South of Barrow broke out at once from 18 June to 19 June (c/r, M) (break-up). Break-up happened during 10 to 15 knot winds from SW.

2005: Thermal break-up on 8 July

Break-up started after landfast sea ice broke out in the Beaufort Sea NE of Point Barrow on 7 July (M), followed by break-out of the ice immediately north of UIC-NARL on 8 July (R). The near-shore landfast sea ice started to drift out to the North at midnight 8 July (w/c), defining break-up. Pressure ridges broke out on 13 July. Break-up happened during westerly winds between 0 and 15 knots, following four hours of winds from SE between 20 and 25 knots.

2006: Thermal break-up on 6 July

Near-shore ice was confined by grounded pressure ridges along the Chukchi Sea coast. Within this confinement, near-shore ice moved along the coast between 3 July and 24 July (M), with break-up (southbound movement) first detected at NARL on 6 July (c/r). Ice drift in the coastal lead was southbound during break-up (c/r). Pressure ridges broke out starting 3 August, and the coast was ice-free by 9 August (M, c/r). Break-up happened during 10 to 15 knot winds from NE.

2007: Mechanical break-up on 27 June

After the landfast ice broke out South of Barrow on 20 June (M), break-out was observed at downtown Barrow and Browerville on 21 June and 23 June, respectively (c/r). Landfast ice broke out at UIC-NARL on 27 June (c/r) (break-up). Only one ice island remained at Browerville and eventually broke out on 2 July (M, c/r). Break-up happened during 15 to 20 knot winds from E.

2008: Thermal break-up on 8 July

With the Chukchi Sea coast heavily ice covered, landfast ice in the Beaufort Sea NE of Point Barrow began to break out around 5 July. Break-up at UIC-NARL occurred on 8 July with northbound movement of near-shore ice along the coast North of Barrow (c/r, A). Break-up at downtown Barrow did not occur until 13 July. Pressure ridges broke out between 17 July and 20 July (c/r). Ice drift in the coastal lead was northbound during break-up (c/r). Break-up occurred while winds decreased from 15 to 10 knots and changed from E to NW.

2009: Thermal break-up on 11 July

Landfast ice was still well in place north of Browerville on 7 July (M). At UIC-NARL, near-shore ice was still present on 9 July, held in place by grounded ridges between Barrow and Point Barrow (E). The near-shore ice was gone by 12 July (M), and grounded ridges gradually broke out or melted until the coast was ice-free by 18 July (M). Break-up occurred with winds of 10 knots from SW. Ice drift in the coastal lead was northbound in early July (c/r, data available until 10 July inclusive). NOAA sealevel measurements at Barrow (station 9494935) indicate that the tidal range was approximately 0.2 m between 9 and 12 July, and the average sealevel decreased by 0.1 m during this period.

2010: Mechanical break-up on 4 July

Coastal ice broke out in segments including both near-shore ice and pressure ridges. Break-out took place at downtown Barrow on 25 June (c/r, w/c) (cf. Figure 12), from downtown Barrow to UIC-NARL on 4 July (c/r, M) (break-up), and North of UIC-NARL up to Point Barrow on 8 July (M, c/r). Some ridged ice remained between UIC-NARL and Point Barrow to break out on 9 July (M). During break-up, winds changed from E to W and N at 10 to 15 knots. Oceanographic measurements are shown in Figure 11 and described in the main body of the paper.

Appendix B

Forecast Irradiance

Our investigations with ARM measurements show that the WRF forecasted irradiance is biased. In order to improve the irradiance forecast we apply an empirical correction as outlined below.

Assuming clouds are conservative scatterers, the fractional downwelling irradiance under a cloud cover is

$$\frac{F_{\downarrow}}{F_0} = \frac{1-\alpha_c}{1-\alpha_g \alpha_c}, \qquad \text{(B1)}$$

where $F_{\downarrow}$ is the downwelling irradiance near ground level, F_0 is the clearsky irradiance, α_g is the ground albedo, and α_c is the effective (cloud cover-averaged) cloud albedo.

We calculate the fractional downwelling irradiance of the WRF model from

$$f = \frac{F_{\downarrow}^{WRF}}{F_0^{est}}, \qquad \text{(B2)}$$

where $F_{\downarrow}^{WRF}$ is the downwelling flux produced by the forecast, and F_0^{est} is the estimated clearsky flux outlined in Equations (B5) – (B7) below. Inverting Equation (B1) and adding an offset, we obtain the effective cloud albedo from

$$\alpha_c = \frac{1-f}{1-\alpha_g^{WRF} f} + \alpha_c^{corr}, \qquad \text{(B3)}$$

where α_g^{WRF} is the assumed ground albedo of the WRF model and α_c^{corr} is an empirical cloud albedo offset.

With the actual ground albedo at the ARM site α_g^{ARM}, we calculate the downwelling forecast irradiance

$$F_{\downarrow}^{FC} = F_0^{est} \frac{1-\alpha_c}{1-\alpha_g^{ARM} \alpha_c}. \qquad \text{(B4)}$$

The parameters used for the irradiance correction are: α_g^{ARM} is 0.6 and 0.2 before and after observed snow melt, respectively, α_g^{WRF} is 0.65 and 0.2 if the ground in the WRF model is ice covered and ice free, respectively, and the offset α_c^{corr} =0.1.

Based on comparison with ARM data, the clearsky irradiance F_0^{est} at Barrow in June and July is estimated based on the solar zenith angle *Z* from

$$F_0^{est} = \Psi\ I_0 \cos(Z), \qquad \text{(B5)}$$

where

$$\cos(Z) = \cos(h)\cos(\delta)\cos(\Phi) + \sin(\delta)\sin(\Phi) \text{ and} \qquad \text{(B6)}$$

$$\delta = -23.45^{o} \cos(360^{o}\ (j+10)/365). \qquad \text{(B7)}$$

Here, h is the local hour angle (0 at noon, 180º at midnight), Φ is the latitude, j is the day of the year, I_0=1368 Wm^{-2} is the solar constant, and Ψ = 0.78 is a calibration constant. If cos(Z)<0 then F_0^{est} is set to 0.

Irradiance Estimate

Due to the delay of the availability of ARM data, the downwelling shortwave flux is estimated from METAR cloud and visibility records. Using Equation (B4), the effective cloud albedo is estimated with the following empirical approach.

$$\alpha_c = \max[\ 0.2,\ (0.5+0.1\ g)\ c_c\ ], \qquad \text{(B8)}$$

where c_c is the effective cloud coverage and g is a weight factor. We set g=0 unless the cloud ceiling is below 2000 ft and the sky condition is either OVC (overcast) or VV (vertical visibility). If the cloud ceiling is below 2000 ft and the sky condition is either OVC or VV, g=1.5 if the visibility is at least 3 miles, and g=5 if the visibility is less than 3 miles. The cloud coverage c_c is calculated assuming random overlap of individual cloud layers, i, specified in the METAR report. Specifically,

$$c_c = 1 - \prod_i (1 - c_c^i), \qquad \text{(B9)}$$

where index i enumerates the cloud layers, and c_c^i is 0, 0.125, 0.375, 0.625 and 1.0 for sky conditions CLR (clear skies), FEW (few clouds), SCT (scattered clouds), BKN (broken cloud cover), and either OVC (overcast) or VV (vertical visibility), respectively. However, above factor c_c^i is reduced by 20% if the ceiling height of layer i is less than 1000 ft.

References

Aagaard, K. and A. T. Roach (1990), Arctic ocean-shelf exchange: Measurements in Barrow Canyon. *J. Geophys. Res., 95*, 18,163–18,175.

Ahlnäs, K. and G. R. Garrison (1984), Satellite and oceanographic observations of the warm coastal current in the Chukchi Sea. *Arctic, 37*, 244-254.

Aporta, C. (2009), The trails as home: Inuit and their pan-Arctic network of routes. *Hum. Ecol., 37*, 131–146.

Barry, R. G., R. E. Moritz, and J. C. Rogers (1979), The fast ice regimes of the Beaufort and Chukchi Sea coasts, Alaska. *Cold Reg. Sci. Technol., 1(2)*, 129–152.

Bilello, M. A. (1980), Decay patterns of fast sea ice in Canada and Alaska. In *Sea ice processes and models: Proceedings of the Arctic Ice Dynamics Joint Experiment (AIDJX) International Commission on Snow and Ice Symposium*, R. S. Prichard (ed), University of Washington Press, Seattle, WA, 313–326.

Bluhm, B., and R. Gradinger (2008), Regional variability in food availability for Arctic marine mammals. *Ecol. Appl., 18*, S77-S96

Chen, F. and J. Dudhia (2001), Coupling an advanced land-surface hydrology model with the PSU/NCAR MM5 modeling system. Part I: Model description and implementation. *Mon. Wea. Rev., 129*, 569–585.

Chou, M.-D., and M. J. Suarez (1994), An efficient thermal infrared radiation parameterization for use in general circulation models. *NASA Tech. Memo. 104606, 3*, 85 pp.

Druckenmiller, M. L., H. Eicken, M. A. Johnson, D. J. Pringle, and C. C. Williams (2009), Toward an integrated coastal sea-ice observatory: System components and a case study at Barrow, Alaska. *Cold Reg. Sci. Technol., 56(2–3)*, 61–72.

Dumas, J. A., G. M. Flato, and R. D. Brown (2006), Future projections of landfast ice thickness and duration in the Canadian Arctic. *J. Climate, 19*, 5175–5189.

Eicken, H., A. L. Lovecraft, and M. L. Druckenmiller (2009), Sea-ice system services: A framework to help identify and meet information needs relevant for Arctic observing networks. *Arctic, 62(2)*, 119-136.

Fox, C. and V. A. Squire (1991), Strain in shore fast ice due to incoming ocean waves and swell, *J. Geophys. Res., 96*, 4531–4547.

Gearheard,S., W. Matumeak, I. Angutikjuaq, J. Maslanik, H. P. Huntington, J. Leavitt, D. Matumeak Kagak, G. Tigullaraq and R. G. Barry (2006), "It's Not That Simple": A collaborative comparison of sea ice environments, their uses, observed changes, and adaptations in Barrow, Alaska, USA, and Clyde River, Nunavut, Canada. *Ambio, 35(4)*, 203–211.

George, J. C., H. P. Huntington, K. Brewster, H. Eicken, D. W. Norton, and R. Glenn (2004), Observations on shorefast ice dynamics in arctic Alaska and the responses of the Iñupiat hunting community. *Arctic, 57(4)*, 363–374.

Grenfell, T. C., and D. K. Perovich (2004), Seasonal and spatial evolution of albedo in a snow-ice-land-ocean environment. *J. Geophys. Res., 109*, C01001, doi:10.1029/2003JC001866.

Gudkovich, Z. M. (1995), Operational tools. *INSROP Working Paper, 10(I.6.1)*, 1-118.

Hume, J. D. and M. Schalk (1967), Shoreline processes near Barrow, Alaska: a comparison of the normal and the catastrophic. *Arctic 20(2)*, 86–103.

Hock, R. (1999), A distributed temperature-index ice- and snowmelt model including potential direct solar radiation. *J. Glaciol. 45(149)*, 101–111.

Johnson, W. R. (1989), Current response to wind in the Chukchi Sea: a regional coastal upwelling event. *J. Geophys. Res., 94*, 2057–2064.

Kniskern, F. E. and G. J. Potocsky (1965), Frost degree day, related ice thickness curves, and harbor freezeup and breakup dates for selected Arctic stations. *Tech. Rep. TR-60*, U. S. Naval Oceanographic Office, 123 pp.

Langhorne, P. J., V. A. Squire, C. Fox, and T. G. Haskell (1998), Breakup of sea ice by ocean waves, *Ann. Glaciol., 27*, 438–442.

Lestak, L. R., W. F. Manley, and J. A. Maslanik (2003), Point Barrow, Alaska, and vicinity bathymetry. Boulder, CO: National Snow and Ice Data Center. Digital media.

Lynch, A. H., L. A. Lestak, P. Uotila, E. N. Cassano, and L. Xie (2008), A factorial analysis of storm surge flooding in Barrow, Alaska. *Monthly Weather Rev., 136*, 898–912.

Mahoney, A., H. Eicken, A. G. Gaylord, and L. Shapiro (2007a), Alaska landfast sea ice: Links with bathymetry and atmospheric circulation. *J. Geophys. Res., 112*, C02001, doi:10.1029/2006JC003559.

Mahoney, A., H. Eicken, and L. Shapiro (2007b), How fast is landfast sea ice? A study of the attachment and detachment of nearshore ice at Barrow, Alaska. *Cold Reg. Sci. Technol., 47(3)*, 233-255.

Mlawer, E. J., S. J. Taubman, P. D. Brown, M. J. Iacono, and S. A. Clough (1997). Radiative transfer for inhomogeneous atmospheres: RRTM, a validated correlated-k model for the longwave. *J. Geophys. Res., 102 (D14)*, 16,663–16,682.

Paquette, R. G., and R. H. Bourke (1981), Ocean circulation and fronts as related to ice melt-back in the Chukchi Sea. *J. Geophys. Res., 86*, 4215-4230.

Petrich, C. and H. Eicken (2010), Growth, Structure and Properties of Sea Ice. In: *Sea Ice, 2nd ed.*, D. N. Thomas and G. S. Dieckmann (eds.), Wiley-Blackwell, Oxford, UK, 23–77.

Perovich, D. K. and G. A. Maykut (1990), Solar Heating of a Stratified Ocean in the Presence of a Static Ice Cover. *J. Geophys. Res., 95(C10)*, 18,233–18,245.

Reimnitz, E., D. Dethleff, and D. Nürnberg (1994), Contrasts in Arctic shelf sea-ice regimes and some implications: Beaufort Sea versus Laptev Sea. *Marine Geol., 119(3–4)*, 215–225.

Reimnitz, E. and D. K. Maurer (1979), Effects of storm surges on the Beaufort Sea coast, northern Alaska. *Arctic, 32(4)*, 329–344.

Rex, R. W. (1955), Microrelief produced by sea ice grounding in the Chukchi Sea near Barrow, Alaska. *Arctic, 8(3)*, 177–186.

Sackinger, W. M. and J. C. Rogers (1974), Dynamics of breakup in shorefast ice. In *Symposium on Beaufort Sea Coast and Shelf Research: Proceedings*, Arctic Institute of North America, Arlington, VA, 367–376.

Shapiro, L. H. and P. W. Barnes (1991), Correlation of nearshore ice movement with seabed ice gouges near Barrow, Alaska. *J. Geophys. Res., 96(C9)*, 16,979–16,989.

Shirasawa, K., M. Lepparanta, T. Saloranta, T. Kawamura, A. Polomoshnov, G. Surkov (2005), The thickness of coastal fast ice in the Sea of Okhotsk. *Cold Reg. Sci. Technol., 42(1)*, 25–40.

Short, A. D., and W. M. J. Wiseman Jr. (1975), Coastal breakup in the Alaskan Arctic. *GSA Bull., 86(2)*, 199–202.

Skamarock, W. C., J. B. Klemp, J. Dudhia, D. O. Gill, D. M. Barker, W. Wang and J. G. Powers (2005), A Description of the Advanced Research WRF Version 2, *NCAR Tech Note, NCAR/TN–468+STR*, 88 pp.

Spedding, L. G. (1983), A large landfast ice movement. In: *Proc. 7th Int. Conf. Port and Ocean Eng. under Arctic Conditions*, Helsinki, Finland, 1983, 203–213.

Spichkin, V. A. (1961), Mechanism of shore ice breakup (in Russian). *Trudy Arkticheskii i antarkticheskii nauchno-issledovatel'skii institut, 256*, 12-27.

Squire, V. A. (2007), Of ocean waves and sea-ice revisited. *Cold Reg. Sci. Technol., 49(2)*, 110–133.

Stone, R. S., E. G. Dutton, J. M. Harris, and D. Longnecker (2002), Earlier spring snowmelt in northern Alaska as an indicator of climate change. *J. Geophys. Res, 107(D10)*, 4089, doi:10.1029/2000JD000286.

U.S. Navy Hydrographic Office (1958) Oceanographic atlas of the polar seas, Part II, Arctic. *H.O. Publication No. 705, Part II*. 149 p.

Weingartner, T.J., D.J. Cavalieri, K. Aagaard, and Y. Sasaki (1998), Circulation, dense water formation, and outflow on the northeast Chukchi shelf. *J. Geophys. Res., 103*, 7647–7661.

Weingartner, T., K. Aagaard, R. Woodgate, S. Danielson, Y. Sasaki, and D. Cavalieri (2005), Circulation on the North Central Chukchi Sea Shelf. *Deep-Sea Res., Pt. II, 52*, 3150-3174.

Woodgate, R. A., K. Aagaard, and T. Weingartner (2005), A Year in the Physical Oceanography of the Chukchi Sea: moored measurements from autumn 1990-91, *Deep-Sea Res., Pt II, 52*, 3116-3149.

Figure captions and Figures

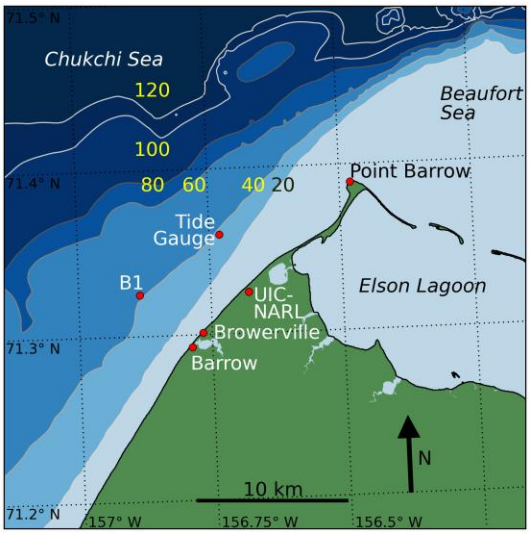

Figure 1. Bathymetric map at Barrow, Alaska. The locations of the 2010 oceanographic mooring B1 and NOAA tide gauge 9494935 are indicated. Bathymetry contours are in meters [*Lestak et al.*, 2003].

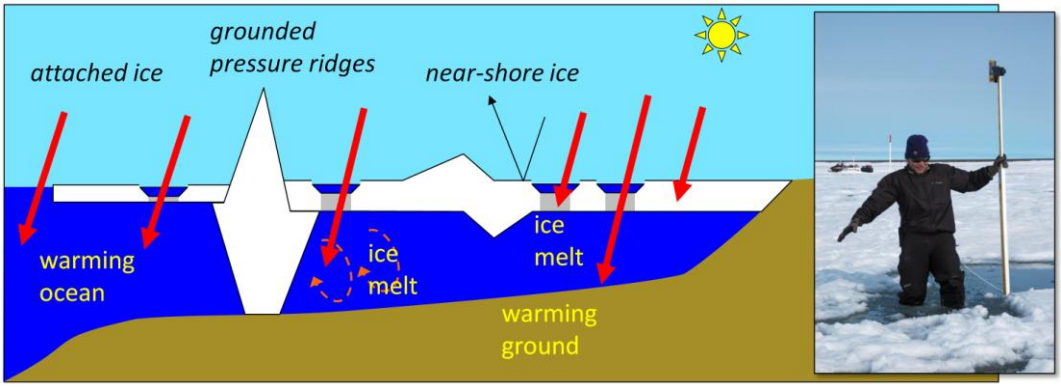

Figure 2. Schematic cross section of landfast ice along the Chukchi Sea coast at Barrow, AK, during the melt season, see text for details. Thick arrows indicate pathways of direct and indirect ice melt from solar radiation. Photo insert illustrates preferential melt under meltponds, 15 June 2009.

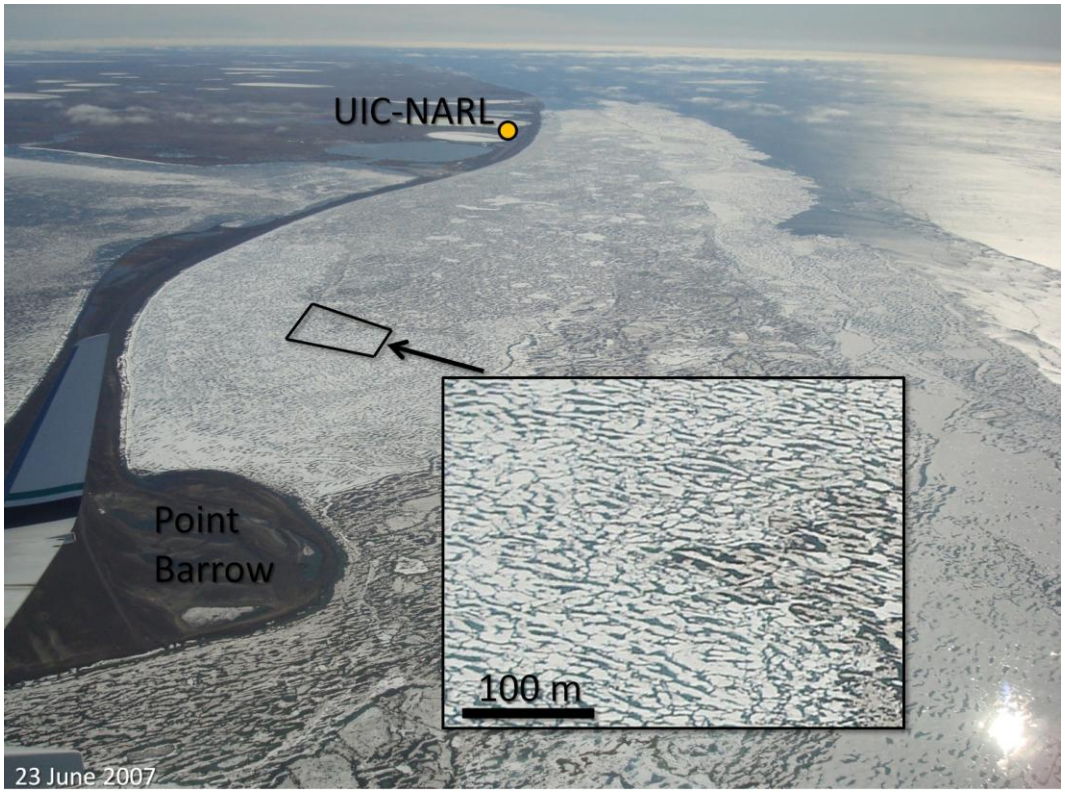

Figure 3. Aerial photograph of landfast ice during the later stages of melt, 23 June 2007, facing South-West with Point Barrow in the foreground. Inset shows interconnected pattern of meltponds.

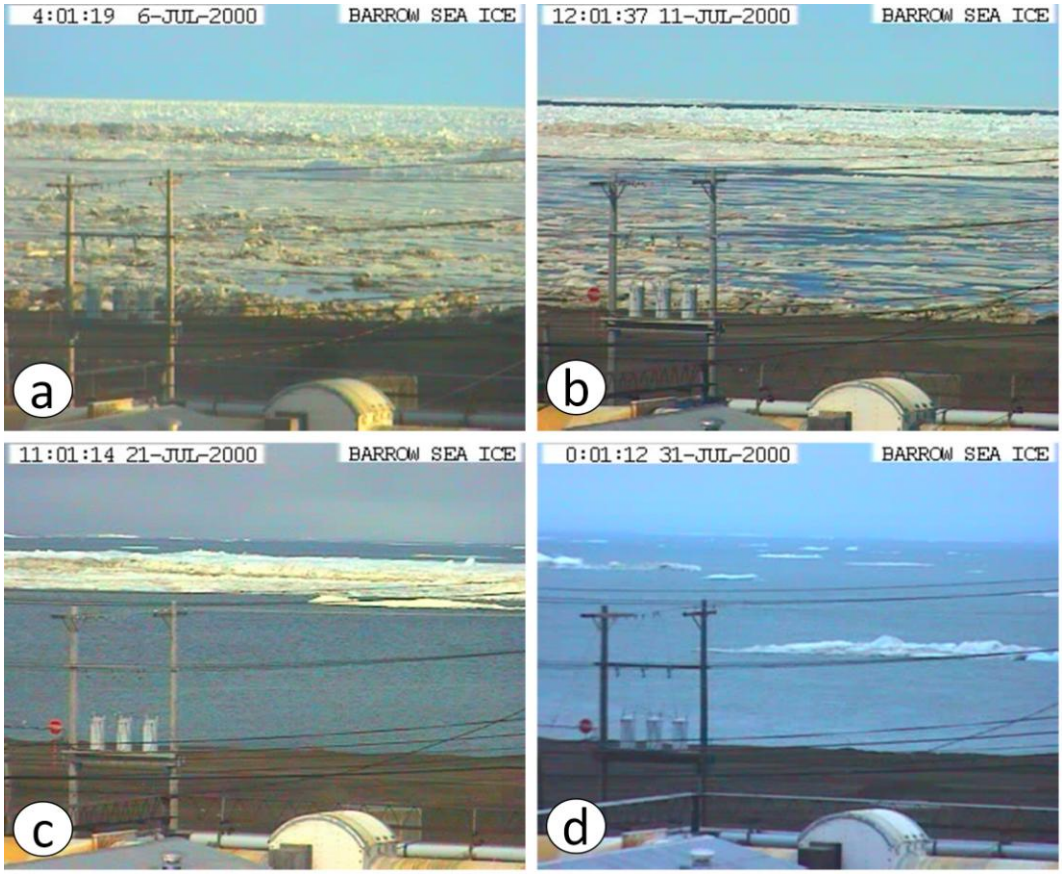

Figure 4. Sequence of webcam images of break-up at UIC-NARL in the summer of 2000. (a) Ice is decaying in place, (b) near-shore ice is moving to the South-West (i.e., to the left), (c) near-shore ice cleared with only grounded ice still in place (1 km off-shore), (d) ice floating at the coast and almost all grounded ice broken out.

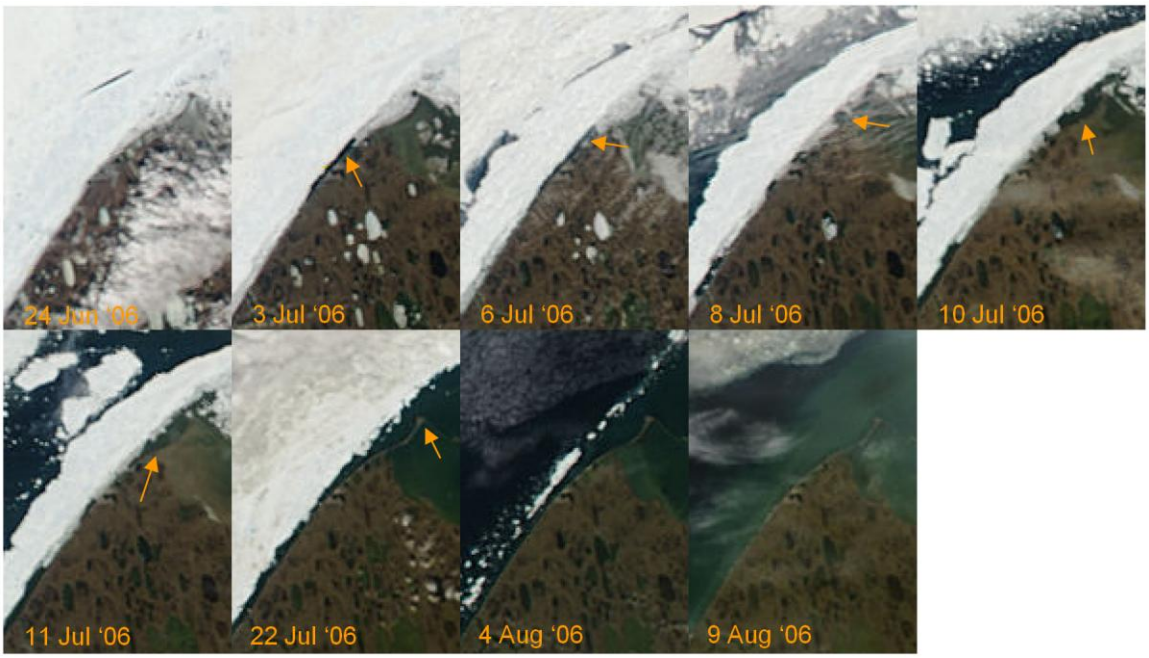

Figure 5. MODIS visible-range composite images for the Barrow region during thermal break-up of 2006. Images show an area approx. 30 km x 40 km in size, pixel resolution is 250 m. Arrows indicate regions of change, see text for detail.

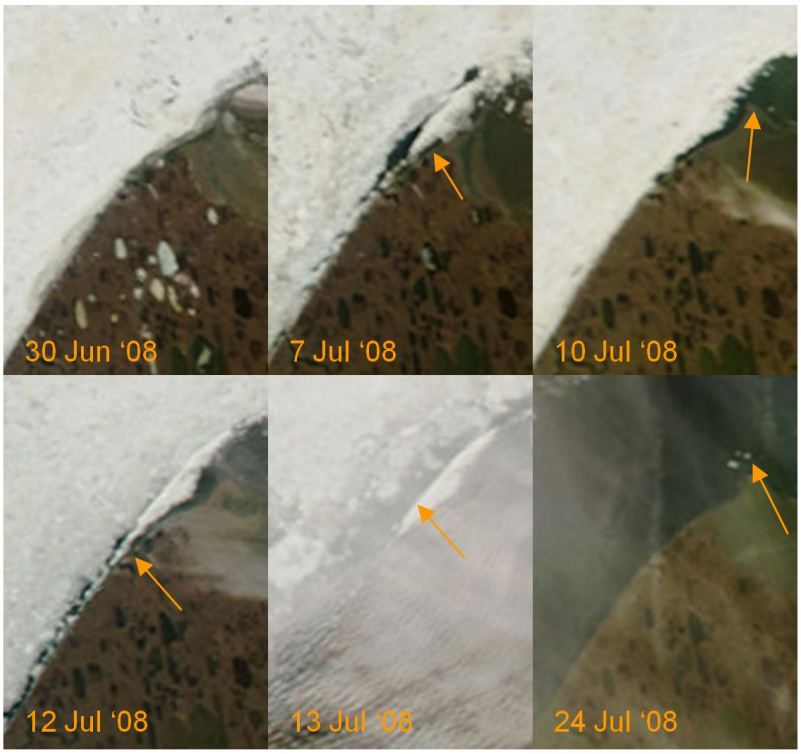

Figure 6. MODIS visible-range composite images for the Barrow region during thermal break-up of 2008. Images show an area approx. 30 km x 40 km in size, pixel resolution is 250 m. Arrows indicate regions of change, see text for detail.

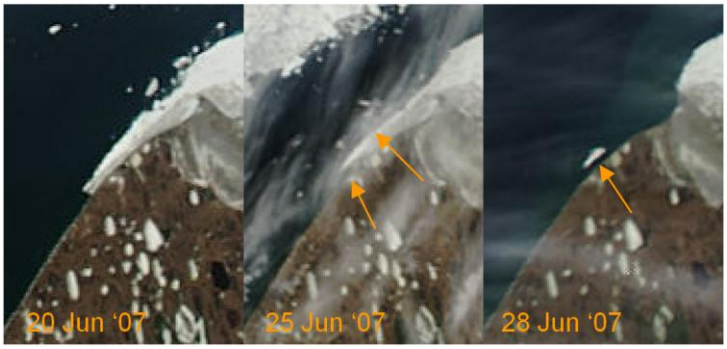

Figure 7. MODIS visible composites near Barrow during mechanical break-up 2007. Images show an area approx. 30 km x 40 km in size, pixel resolution is 250 m. Arrows indicate regions of change, see text for detail.

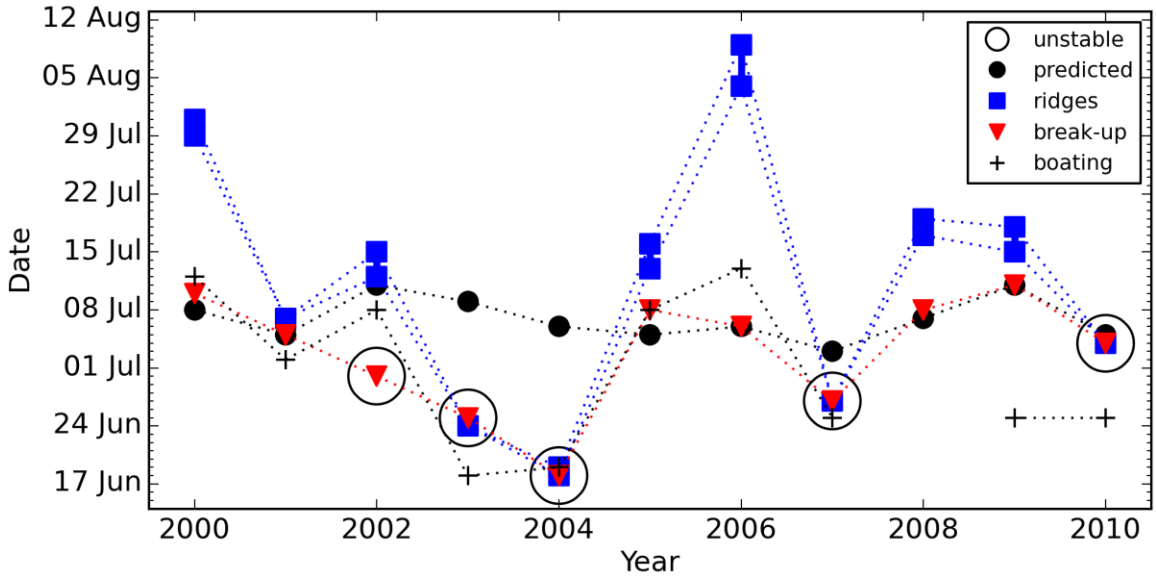

Figure 8. Comparison of break-up dates at UIC-NARL (triangles) and movement of pressure ridges (squares) with predicted break-up dates, assuming thermal break-up (dots) and the start of local boating activity (pluses). Break-up in years circled was mechanical (unstable) rather than thermal.

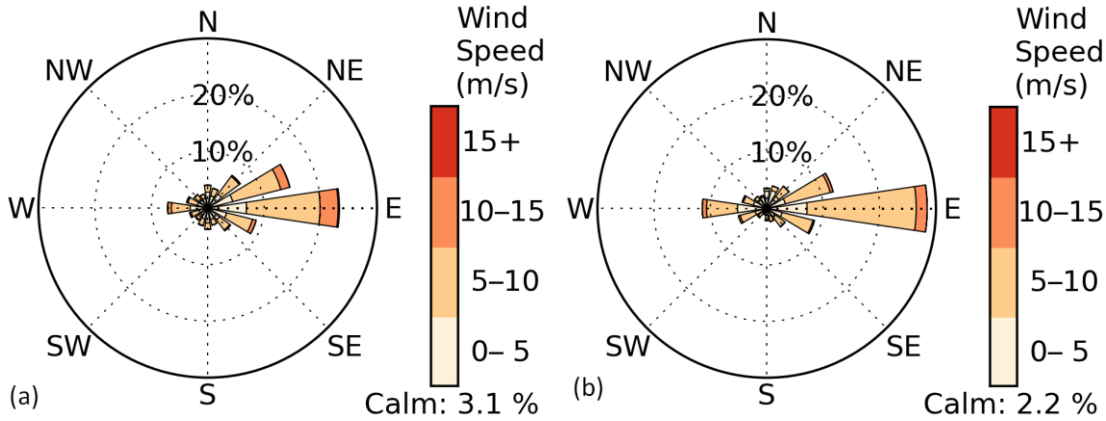

Figure 9. Wind rose for Barrow airport (a) 2000 through 2010, and (b) only June and July of 2000 through 2010.

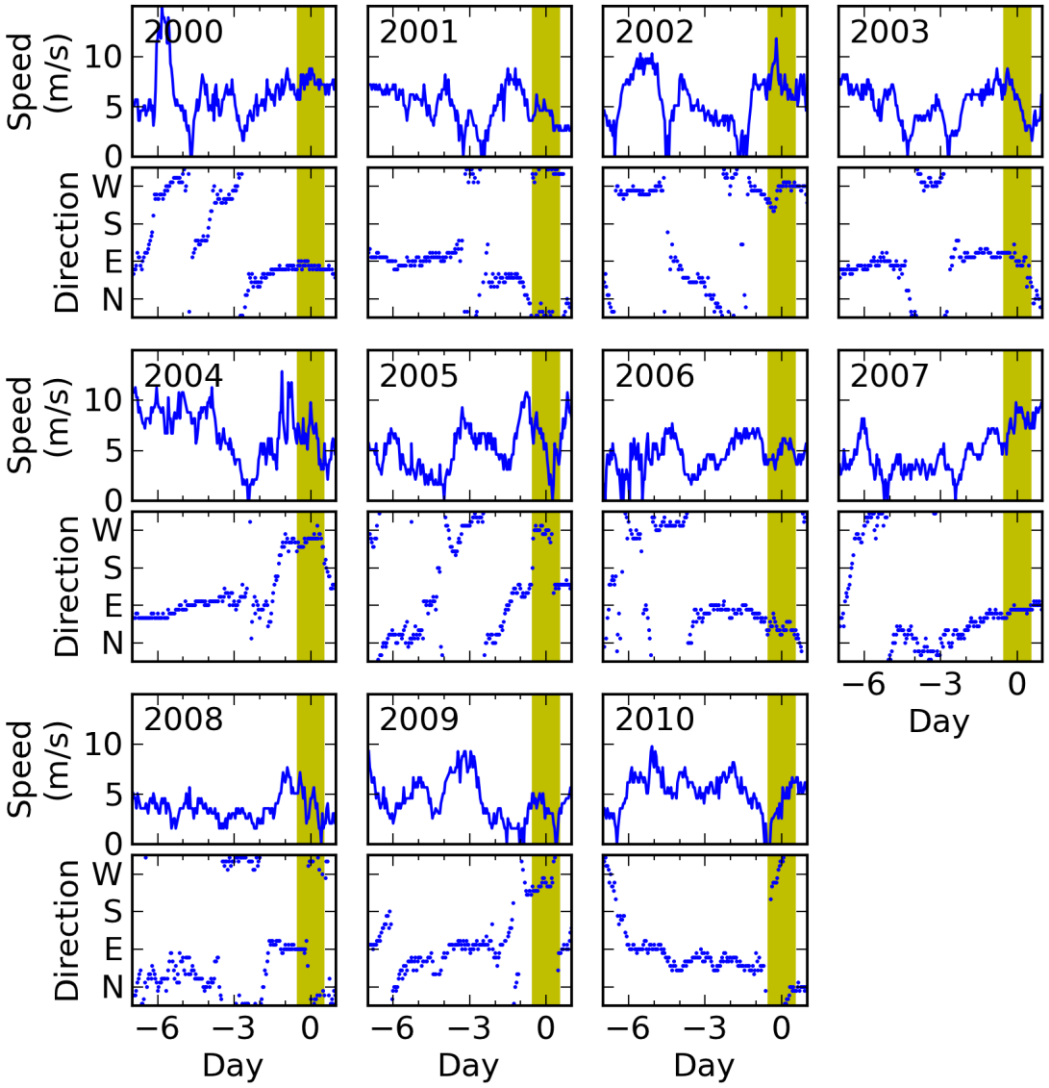

Figure 10. Winds at Barrow during break-up. Day 0 is local noon on the day of break-up (Table 1), the shaded area covers ±12 hours.

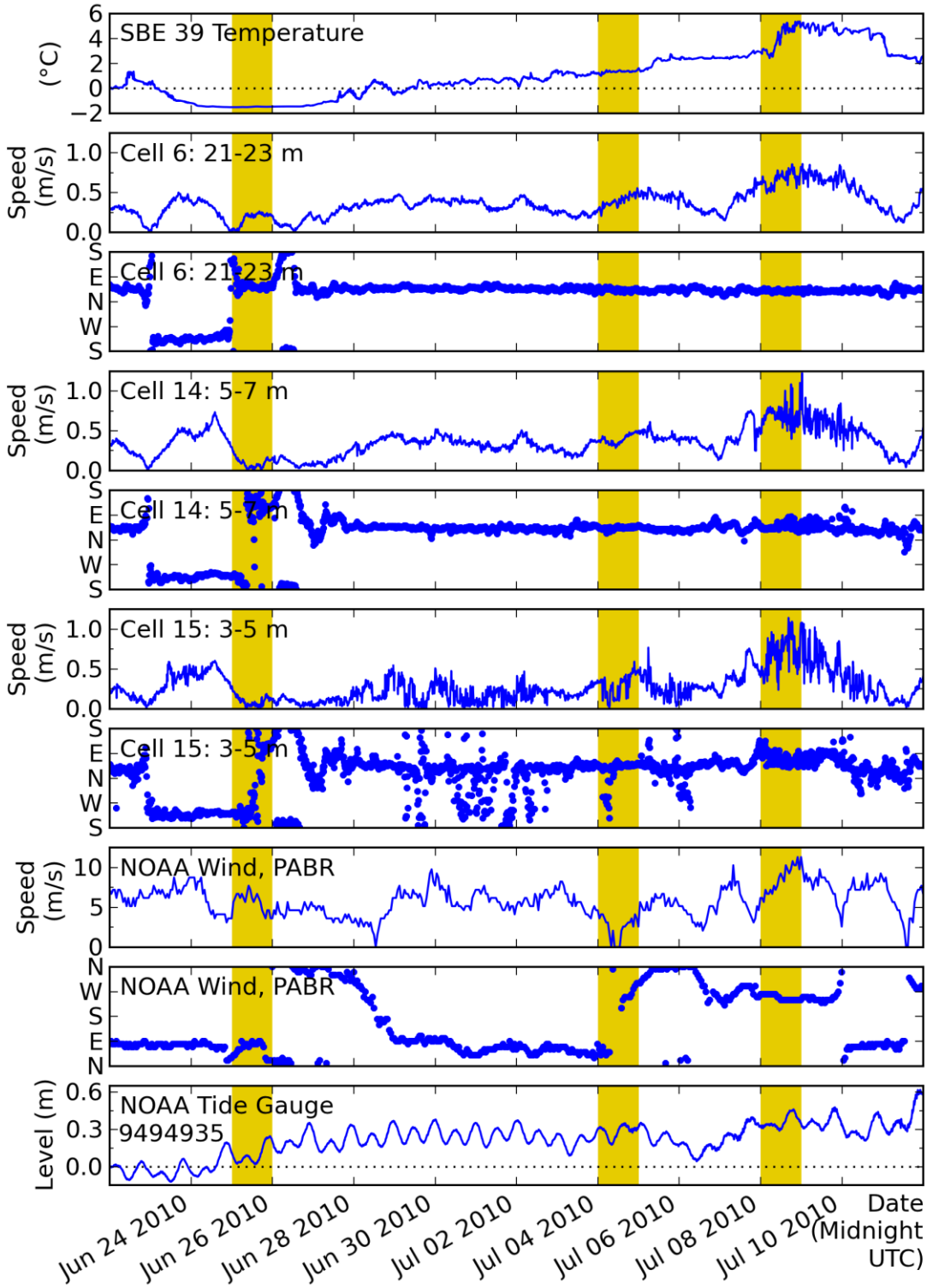

Figure 11. Ocean and weather data near UIC-NARL for the break-up season in 2010. Direction of currents and winds are the direction of movement towards and from, respectively. Sealevel is given relative to mean lower low-water (MLLW). Shaded areas highlight two notable break-out events (25 June, 8 July) and break-up (4 July).

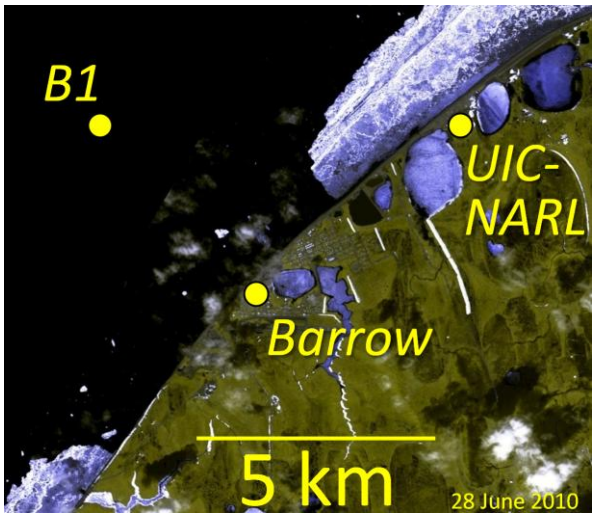

Figure 12. ALOS AVNIR-2 false-color image at Barrow on 28 June 2010, nadir-looking. Ice and clouds are bluish–white. *B1* is the location of the mooring. Landfast ice has broken out within approximately 3 km of downtown Barrow.

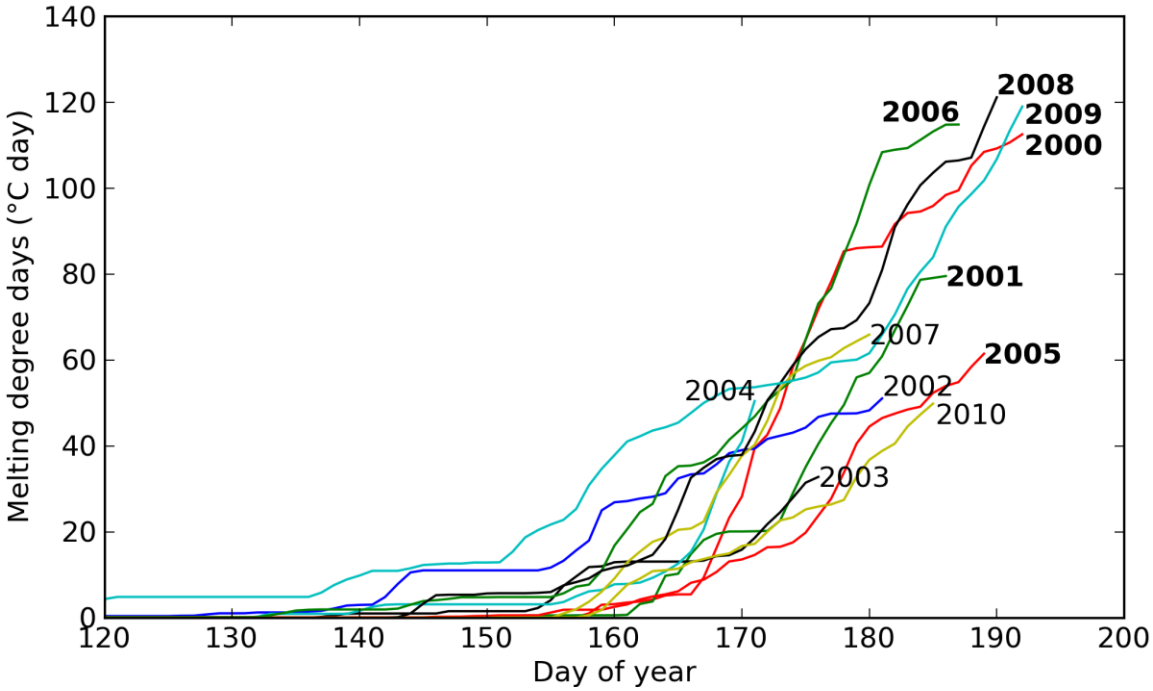

Figure 13. Annual, cumulative melting degree days until break-up. Bold years indicate thermal break-up.

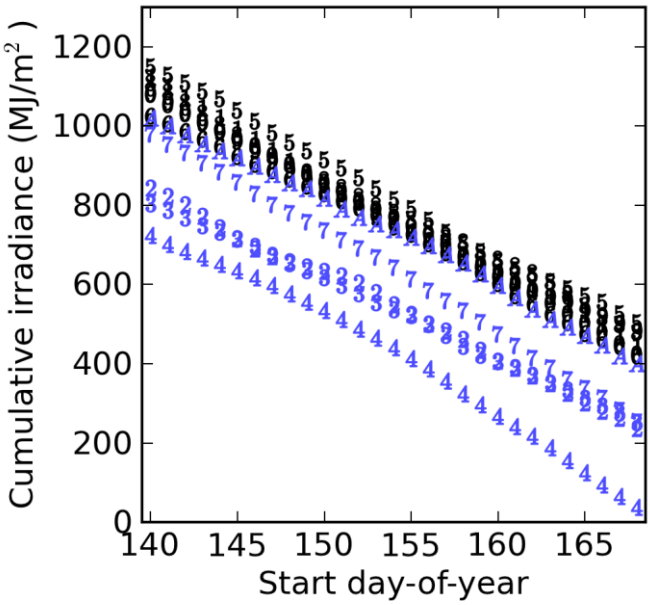

Figure 14. Cumulative irradiance until observed break-up for different start dates of integration. Markers are the last digit of the year from 2000 to 2009, with "A" denoting 2010. Black markers are years of thermal break-up.

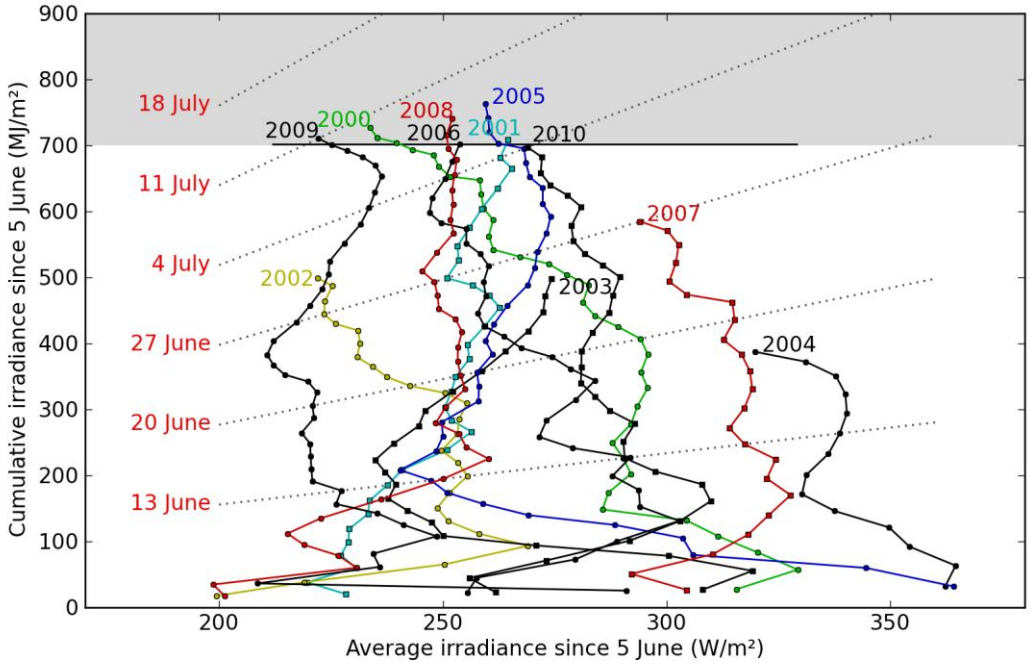

Figure 15. Trajectories of cumulative irradiance versus average irradiance measured at the ARM site between 5 June and break-up.

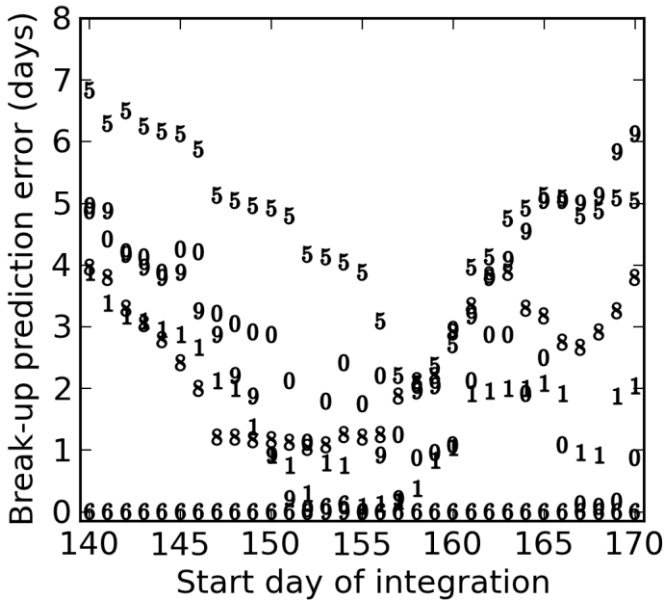

Figure 16. Range of errors in break-up prediction for various integration start dates for years of thermal break-up (Table 1).

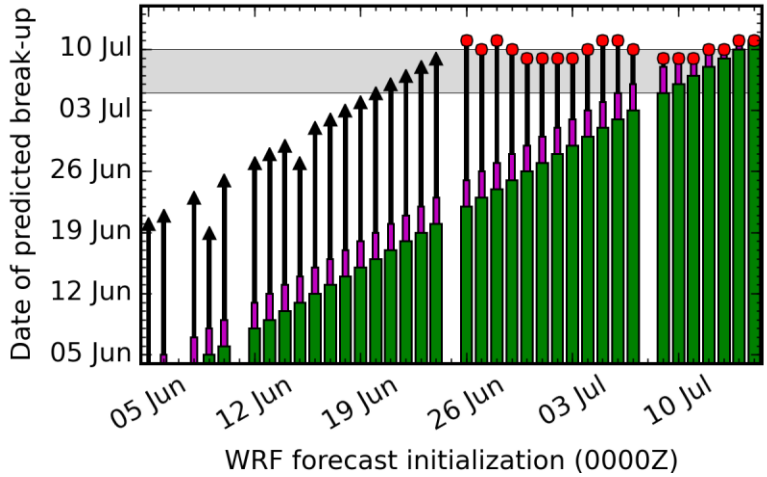

Figure 17. Date of break-up forecast for 2009 versus initialization time of the WRF model. Circles indicate the expected break-up dates, triangles indicate the end of a WRF forecast run without expected break-up. The vertical bars indicate the data source for the incoming shortwave flux, i.e., ARM measurements (thick vertical bars, green), estimates based on observed cloud cover (medium thick vertical bars, magenta) and WRF runs (thin vertical bars, black). The shaded horizontal bar indicates the range of thermal break-up dates 2000–2008.

Tables

Table 1. Break-up mode and timing, melting degree days (MDD) at break-up, and cumulative irradiance at break-up, starting integration on 5 June

Year	Near-shore ice mode	starting	Pressure ridges period	MDD (°C days)	Cumulative Irradiance (MJ/m^2)
2000	thermal	10 July	29–31 July	113	700
2001	thermal	5 July	7 July	80	710
2002	*	30 June	1–15 July	51	499
2003	mechanical	25 June	24 June	33	498
2004	mechanical	18 June	18 June	50	356
2005	thermal	8 July	13–16 July	62	762
2006	thermal	6 July	4–9 August	115	701
2007	mechanical	27 June	27 June	66	584
2008	thermal	8 July	17–19 July	121	723
2009	thermal	11 July	15–18 July	119	711
2010	mechanical	4 July	4 July	50	697

* See Section 4 for 2002